

Variational Quantum Algorithm for Non-equilibrium Steady States

Nobuyuki Yoshioka^{1,*}, Yuya O. Nakagawa², Kosuke Mitarai^{2,3}, and Keisuke Fujii^{3,4}

¹*Department of Physics, University of Tokyo, 7-3-1 Hongo, Bunkyo-ku, Tokyo 113-0033, Japan*

²*QunaSys Inc., High-tech Hongo Building 1F, 5-25-18 Hongo, Bunkyo, Tokyo 113-0033, Japan.*

³*Graduate School of Engineering Science, Osaka University,*

1-3 Machikaneyama, Toyonaka, Osaka 560-8531, Japan. and

⁴*JST, PRESTO, 4-1-8 Honcho, Kawaguchi, Saitama 332-0012, Japan.*

(Dated: June 18, 2022)

We propose a quantum-classical hybrid algorithm to simulate the non-equilibrium steady state of an open quantum many-body system, named the dissipative-system Variational Quantum Eigensolver (dVQE). To employ the variational optimization technique for a unitary quantum circuit, we map a mixed state into a pure state with a doubled number of qubits and design the unitary quantum circuit to fulfill the requirements for a density matrix. This allows us to define a cost function that consists of the time evolution generator of the quantum master equation. Evaluation of physical observables is, in turn, carried out by a quantum circuit with the original number of qubits. We demonstrate our dVQE scheme by both numerical simulation on a classical computer and actual quantum simulation that makes use of the device provided in Rigetti Quantum Cloud Service.

I. INTRODUCTION

Technological developments in quantum devices have now reached a stage to realize the near-term quantum computers that contain from tens to hundreds of qubits with high gate fidelity, although their qubits are prone to error (or not fault-tolerant) [1–3]. Such quantum computers are dubbed as the Noisy Intermediate-Scale Quantum (NISQ) devices [4]. Even though their rigorous computational speedup is still obscured, it is becoming practically impossible to simulate the NISQ devices by classical computers [5–11]. This triggers a surging interest in utilizing the NISQ devices for various kinds of problems in the real world: the simulations of quantum many-body systems including their dynamics [12], quantum chemistry calculations [13], combinatorial optimization problems [14], and so on.

In particular, intriguing research field among the proposed applications of the near-term quantum computers are the Variational Quantum Eigensolver (VQE) scheme [15] and its variants. Originally proposed for obtaining the ground state and its energy of a given Hamiltonian, the extensions of the VQE scheme are also capable of the excited states and their energies [16–21]. So far, such developments including actual quantum simulations [22–25] focus only on *closed* quantum systems, which is a system that does not exchange energy with its external environment. Physical systems in reality inevitably interact with their environment, and full understanding of such quantum phenomena is essential, e.g., for exploring the rich nature at out-of-equilibrium and designing quantum information processing devices.

A particularly significant topic is the non-equilibrium steady state (NESS) under time-independent dissipation [26–37]. For instance, it has been shown that prop-

erly engineered dissipations can stabilize intriguing quantum states that are topologically nontrivial [38] or useful for measurement-based quantum computation [39, 40]. Also, the transport property of the NESS in nano-scale devices such as single-atom junctions is an important topic [41]. Such surging interests in the totally new regime due to the variety of behaviors are also reflected in the development of variational approaches for the NESS based on, e.g., tensor network techniques [26–29] and neural networks [30–33]. We note that several proposals on the NISQ devices consider open systems [42–44], but their focuses are on the dynamics and no direct treatment of the NESS has been presented.

In this paper, we propose a scheme to calculate the NESS of a given open system by using the methodology of the VQE. The proposed method, which we refer to as the dissipative-system VQE (dVQE), allows one to variationally determine the NESS of the system by minimizing a bounded cost function that is closely related with the accuracy of the optimization. To satisfy the necessary conditions required for mixed quantum states, a sophisticated ansatz, which uses doubled number of qubits to map a mixed state into a pure state, is employed in the dVQE scheme. Since a naive procedure to calculate the physical observables for the NESS becomes exponentially inefficient as the number of qubits increases, a measurement technique is introduced to avoid this problem. We demonstrate our dVQE scheme by two styles of simulation; one is performed solely on a classical computer [45], and another is executed in actual quantum-classical hybrid manner that makes use of the NISQ device provided in Rigetti Quantum Cloud Service [46]. Our proposal would open up the possibility of the NISQ devices to explore the rich field of open quantum systems.

The remainder of the paper is organized as follows. In Sec. II, we introduce the time independent quantum master equation for mixed states. In particular, the generator of the time evolution, or the Liouvillian, for the

* nysocloud@g.ecc.u-tokyo.ac.jp

vectorized expression of the density matrix is discussed. We map the problem of searching the non-equilibrium steady state into an optimization problem in Sec. III, and also discuss the appropriate variational quantum circuit and measurement scheme for the density matrix. After we provide both numerical and experimental demonstrations of our dVQE scheme in Sec. IV, we present conclusion and discussion in Sec. V. For completeness, we discuss algorithm of the sequential minimal optimization method [47] in Appendix A. The procedure to mitigate the gate error in the quantum circuit is provided in Appendix B.

II. EQUIVALENT REPRESENTATIONS OF QUANTUM MASTER EQUATION

Among the numerous schemes that treat the continuous-time open quantum systems, here we choose the standard formalism which is described by the homogeneous Markovian master equation. Such evolution of a mixed state ρ , which is assured to fulfill the completely-positive and trace-preserving property, is governed by the so-called Gorini-Kossakowski-Sudarshan-Lindblad (GKSL) equation [48, 49] or equivalently the ordinary quantum master equation of the Lindblad type. In the following, we give the expression of the GKSL equation in two equivalent ways: the matrix and vector representations. The former is the originally proposed quantum master equation for the density matrix, and the latter, initially adopted by Ref. [27] to obtain the NESS variationally, maps density matrix into a pure state with doubled number of qubits.

A. Matrix representation

First, we introduce the ordinary matrix representation of the GKSL equation. The Liouvillian superoperator $\mathcal{L} : \mathcal{H} \otimes \mathcal{H} \rightarrow \mathcal{H} \otimes \mathcal{H}$ for the finite-dimensional Hilbert space \mathcal{H} governs the time evolution as follows,

$$\dot{\rho} = \mathcal{L}\rho := -i[H, \rho] + \sum_k \frac{\gamma_k}{2} \mathcal{D}[c_k]\rho, \quad (1)$$

where the commutator in the right-hand side, $[A, B] = AB - BA$, describes unitary part of the dynamics given by the Hamiltonian of the system $H : \mathcal{H} \rightarrow \mathcal{H}$. The second term with dissipation amplitude γ_k destroys the coherence of the pure states in general, governed by a superoperator $\mathcal{D}[c_k] : \mathcal{H} \otimes \mathcal{H} \rightarrow \mathcal{H} \otimes \mathcal{H}$ that acts on an operator as

$$\mathcal{D}[c_k]\rho = c_k \rho c_k^\dagger - \frac{1}{2} \left\{ c_k^\dagger c_k, \rho \right\}, \quad (2)$$

where c_k is the k -th jump operator which determines the detail of dissipation. In the following, we consider time-independent Liouvillian superoperator which has at least

one steady state that satisfies

$$\mathcal{L}\rho_{\text{SS}} = 0, \quad (3)$$

where ρ_{SS} denotes the density matrix of the NESS [50].

B. Vector representation

Although universal quantum computers may simulate completely-positive and trace-preserving maps so that the time evolution of quantum open systems can be studied, this is not the case for the NISQ devices as same as simulation of Hamiltonian dynamics. Therefore, we discuss the equivalent formalism for the GKSL equation in which density “matrix” $\rho : \mathcal{H} \rightarrow \mathcal{H}$ is mapped to a “vector,” namely a pure state in the Hilbert space with doubled number of qubits as $|\rho\rangle \in \mathcal{H} \otimes \mathcal{H}$. Concretely, the mapping is given as

$$\rho = \sum_{ij} \rho_{ij} |i\rangle \langle j| \mapsto |\rho\rangle = \sum_{ij} \frac{\rho_{ij}}{C} |i\rangle_{\mathcal{P}} \otimes |j\rangle_{\mathcal{A}}, \quad (4)$$

where the factor $C = \sqrt{\sum_{ij} |\rho_{ij}|^2}$ assures the norm of the state to be unity. Note that such a mapping is essential in application of the NISQ devices which is, in general, only capable of unitary operations on pure states. Here, we discriminate the qubits that correspond to the ket and bra in the matrix representation by referring to as the physical and ancillary qubits, respectively. This is also reflected on the subscripts \mathcal{P} and \mathcal{A} . Although two representations of GKSL equation yield identical results, we emphasize that the normalization of states differs from each other; the trace of the matrix is set to unity in the matrix representation, i.e., $\sum_i \rho_{ii} = 1$, while the L_2 norm of $|\rho\rangle$ is unity in the vector representation.

Under the mapping defined in Eq. (4), the Liouvillian superoperator acts as linear operator on the Hilbert space with doubled number of qubits. Such generator in the vector representation $\hat{\mathcal{L}} : (\mathcal{H} \otimes \mathcal{H} \rightarrow \mathcal{H} \otimes \mathcal{H})$, dubbed as the Liouvillian operator in the following, acts on a state $|\rho\rangle$ as

$$\hat{\mathcal{L}}|\rho\rangle = \left(-i(H \otimes \mathbb{1} - \mathbb{1} \otimes H^T) + \sum_k \hat{\mathcal{D}}[c_k] \right) |\rho\rangle, \quad (5)$$

$$\hat{\mathcal{D}}[c_k] = \frac{\gamma_k}{2} \left(c_k \otimes c_k^* - \frac{1}{2} c_k^\dagger c_k \otimes \mathbb{1} - \mathbb{1} \otimes \frac{1}{2} c_k^T c_k^* \right), \quad (6)$$

where $*$ denotes the complex conjugate. This can be derived by utilizing the mapping of operations that act from left and right of the density matrix as

$$A\rho B \mapsto |A\rho B\rangle = A \otimes B^T |\rho\rangle. \quad (7)$$

Using the new representation, the problem of finding the NESS is expressed in terms of standard linear algebra. Concretely, our goal is to solve the following equation for non-hermitian operator $\hat{\mathcal{L}}$ given as

$$\hat{\mathcal{L}}|\rho_{\text{SS}}\rangle = 0. \quad (8)$$

Note that we may also formalize the problem using the purification of the mixed state. In such a case, we search for the state which is invariant under the non-unitary time evolution generated by the Liouvillian superoperator. However, it is non-trivial whether such time evolution operation could be expressed efficiently by local operators, and therefore we employ the vector representation in the present work.

III. METHOD

In the following, we introduce the dVQE scheme to simulate the NESS and its physical observables in open quantum systems. This is done by firstly casting the problem of finding the NESS into an optimization problem of an appropriate Hermitian operator in the vector representation. Next, the structure of the variational quantum circuit suited to express the density matrix in the vector representation is provided, and finally the measurement procedure for the physical observables in the original matrix representation is discussed. Such modification of the representation is crucial to execute proper calculation.

A. Searching NESS by variational optimization

The Liouvillian operator defined as Eq. (6) is in general a non-hermitian matrix. If the dissipation is absent or parity-time symmetric [51], the Liouvillian operator is skew hermitian, and therefore is diagonalizable by an unitary matrix to obtain pure imaginary eigenvalues. If it is not the case, which is the target in this work, the eigenvalues are neither purely real nor imaginary in general, and the eigenmodes are not orthogonal.

In contrast, the product with the adjoint of the Liouvillian operator, $\hat{\mathcal{L}}^\dagger \hat{\mathcal{L}}$, is a Hermitian matrix with non-negative spectrum. Obviously, the eigenstate(s) with lowest eigenvalue(s) $\lambda = 0$ correspond to the NESS, i.e., the NESS $|\rho_{\text{SS}}\rangle$ satisfies

$$\hat{\mathcal{L}}^\dagger \hat{\mathcal{L}} |\rho_{\text{SS}}\rangle = 0. \quad (9)$$

In the following, we exclusively consider models that can be shown to have unique NESS [52] so that the ground-state-search techniques for the variational quantum circuit can be applied. In the dVQE scheme, we employ the expectation value of $\hat{\mathcal{L}}^\dagger \hat{\mathcal{L}}$ as the cost function. The parameters in the ansatz are optimized to reach the minimal value of the cost function which is lower-bounded by zero [53]. While the lower bounded property of the cost function, $\hat{\mathcal{L}}^\dagger \hat{\mathcal{L}}$, gives us information on the quality of the optimization [54], one must be aware of the difference of the normalization between the matrix and vector representation when one sets the desirable value of the cost function.

Note that the dVQE scheme can be straightforwardly extended to models with multiple NESSs by using the

VQE methods that deal with excited states [16–21]. In general, the largest or smallest singular values of an operator given by a sum of local operator can be obtained by the proposed method.

The task of optimization is divided into two processing units; the QPU (quantum processing unit) carries the quantum state while the CPU executes the optimization of the variational parameter based on the measurement result in the QPU [15]. A quantum-classical hybrid approach designed for open quantum systems can be summarized as follows.

1. Initialize the variational parameters of the ansatz $U(\theta)$.
2. QPU part: Estimate the cost function $\langle \hat{\mathcal{L}}^\dagger \hat{\mathcal{L}} \rangle$ by sampling from the quantum state given by the variational quantum circuit as $|\rho_\theta\rangle = U(\theta) |0\rangle^{\otimes 2N}$.
3. CPU part: Based on the measurement results in QPU, compute the new parameters θ' using a classical optimization technique and replace θ .
4. Repeat 2 and 3 until the cost function converges.

B. Ansatz for dVQE

In the following, we introduce an variational quantum circuit to represent the NESS in the vector representation, which, as we have seen in §III A, enables us to execute the optimization in a parallel fashion with the VQE for closed systems [15]. Note, however, that the following conditions are required for the density matrix ρ to be physical:

- (I) $\rho^\dagger = \rho$ (Hermiticity),
- (II) $\langle \psi | \rho | \psi \rangle \geq 0, \forall |\psi\rangle \in \mathcal{H}$ (Positive semi-definiteness),
- (III) $\text{Tr}[\rho] = 1$ (Unit trace).

As we describe in the following, our dVQE scheme satisfies all the conditions. It suffices to consider the condition (III) only when we measure the expectation value of physical observables; the normalization of the representation can be neglected during the optimization without affecting the accuracy of the optimization. In the following, we discuss how to design an appropriate ansatz to satisfy the conditions (I) and (II).

We first diagonalize the density matrix ρ using unitary matrix. Let q_k be the k -th bit that takes either 0 or 1 and $\mathbf{q} = (q_1, \dots, q_N)$ be an array of N bits, and we decompose the density matrix as

$$\rho = V D V^\dagger, \quad (10)$$

$$D = \text{diag}(\{\lambda_{\mathbf{q}}\}). \quad (11)$$

Here, D gives the eigenvalue distribution, which are related to the entropy of the state, and V corresponds to

the basis transformation that generates quantum entanglement between qubits. As is graphically described in Fig. 1, the vector representation of Eq. (10) is given by using the mapping given by Eq. (7) as

$$|\rho\rangle = [V \otimes V^*] |D\rangle \quad (12)$$

where the eigenvalue distribution is expressed as

$$\begin{aligned} |D\rangle &= \sum_{\mathbf{q}} \frac{\lambda_{\mathbf{q}}}{C} |\mathbf{q}\rangle_{\mathcal{P}} \otimes |\mathbf{q}\rangle_{\mathcal{A}} \\ &= \left(\prod_{n=1}^N \text{CNOT}_{n,n+N} \right) \sum_{\mathbf{q}} \frac{\lambda_{\mathbf{q}}}{C} |\mathbf{q}\rangle_{\mathcal{P}} \otimes |0\rangle_{\mathcal{A}}, \quad (13) \\ &= \left(\prod_{n=1}^N \text{CNOT}_{n,n+N} \right) \tilde{D} |0\rangle_{\mathcal{P}} \otimes |0\rangle_{\mathcal{A}}. \quad (14) \end{aligned}$$

Here, CNOT gates operating on the n -th and $(n+N)$ -th qubits, which are taken as the control and target qubits, respectively, entangle the left and right space such that the matrix representation of the state yields a diagonal matrix. Viewed in the computational basis, CNOT gate is concretely expressed as

$$\begin{aligned} \text{CNOT} &= |0\rangle\langle 0| \otimes (|0\rangle\langle 0| + |1\rangle\langle 1|) + \\ &\quad |1\rangle\langle 1| \otimes (|0\rangle\langle 1| + |1\rangle\langle 0|), \quad (15) \end{aligned}$$

where the first and second qubits denote the control and target qubits.

We propose an ansatz based on Eq. (10) as

$$|\rho_{\theta}\rangle = U(\theta) |0\rangle \quad (16)$$

$$\begin{aligned} &= [V(\theta_v) \otimes V^*(\theta_v)] \\ &\quad \times \left(\prod_{n=1}^N \text{CNOT}_{n,n+N} \right) \tilde{D}(\theta_d) |0\rangle, \quad (17) \end{aligned}$$

where $U(\theta)$ is the ansatz for the NESS that consists of quantum circuit $\tilde{D}(\theta_d)$ ($V(\theta_v)$) for the eigenvalue distribution (basis transformation) parametrized by a set of R_d (R_v) values, i.e., $\theta_d := \{\theta_d^r\}_{r=1}^{R_d}$ ($\theta_v := \{\theta_v^r\}_{r=1}^{R_v}$). Here, the union of the variational parameters are denoted as $\theta = \theta_d \cup \theta_v$. The matrix representation of a state given by Eq. (17) automatically fulfills the condition (I), and also the condition (II) can be satisfied by imposing appropriate restriction on the parameters θ_v .

Shown in Figs. 2 and 3 are concrete examples for $\tilde{D}(\theta_d)$ and $V(\theta_v)$, respectively. For the eigenvalue distribution, we consider two structures: one with repeating structure of single-qubit and controlled Y rotations and another with solely the single-qubit Y rotation. Such quantum circuit, graphically shown in Fig. 2 (a) and (b), respectively, are referred to as the “entangled type” and “decoupled type” in the following. Here, the unitary gate for the rotation along a -axis is given as $e^{-ia\theta/2}$ where θ denotes the angle. For the basis transformation, we adopt the so-called hardware-efficient ansatz [24], in which the block consisting of an arbitrary single-qubit gate for each qubit and CZ gates between neighboring qubits are repeated.

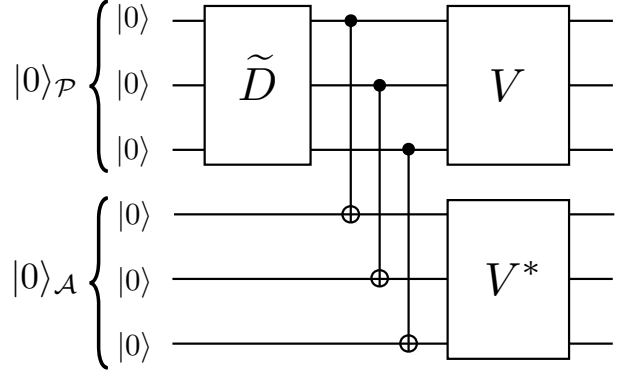


FIG. 1. (Color Online) Variational quantum circuit as the ansatz for the vector representation of the NESS of open quantum system with 3 physical qubits. Both the physical and ancillary qubits, denoted as $|0\rangle_{\mathcal{P}}$ and $|0\rangle_{\mathcal{A}}$ respectively, are initialized to zero. To impose the Hermiticity and positive-semidefiniteness that are required for density matrices, quantum gates for eigenvalue distribution \tilde{D} , CNOT gates between physical and ancillary qubits, and basis transformation V operate sequentially.

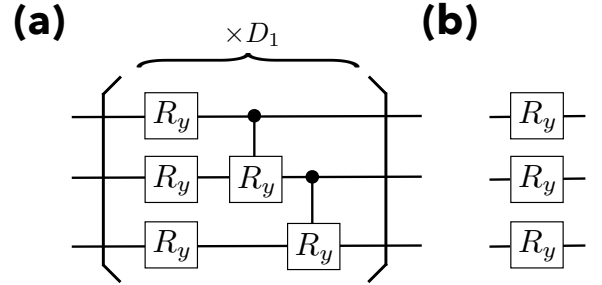


FIG. 2. (Color Online) Examples for the quantum circuit for eigenvalue distribution \tilde{D} . (a) The entangled type which consists of the repeating structure of single-qubit gates and controlled Y rotation. Here, D_1 denotes the repetition of the block in the bracket to enhance the representability of the ansatz. (b) The decoupled type with solely the single-qubit Y rotations.

C. Measurement of physical observables

After the optimization scheme proposed in Sec. III A has been executed for the variational quantum circuit introduced in Sec. III B, our interest would be focused on the measurement of physical observable for the NESS.

Note that the vector representation is not appropriate when evaluating observables. Any measurement of an observable defined on a state $|\rho\rangle = \sum_{ij} \frac{\rho_{ij}}{C} |i\rangle_{\mathcal{P}} |j\rangle_{\mathcal{A}}$ that represents a density matrix ρ would involve products of the coefficients ρ_{ij} , which is incompatible to, for example, the expression of an expectation value of a physical observable O computed as $\text{Tr}(\rho O)$.

To avoid the above-mentioned problem, we map the optimized ansatz into the matrix representation which

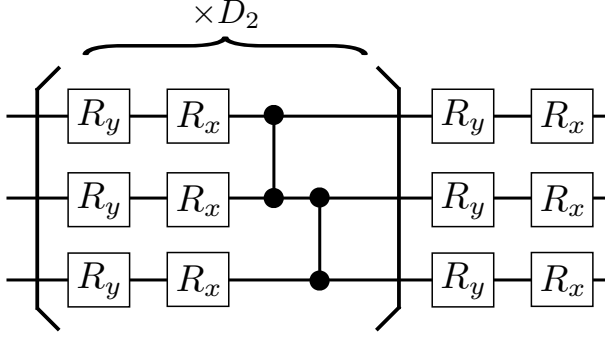


FIG. 3. (Color Online) Example for the quantum circuit for the basis transformation V . Here, we adopt the so-called hardware-efficient ansatz which repeats the block consisting of an arbitrary single-qubit gate for each qubit and CZ gates between neighboring qubits. The repetition number of the block in the bracket is denoted as D_2 .

requires only N qubits instead of $2N$ qubits. With the dependence on the variational parameters abbreviated for simplicity, the optimized ansatz is mapped from $|\rho\rangle = [V \otimes V^*] \tilde{D} |0\rangle$ into $\rho = \sum_{\mathbf{q}} \lambda_{\mathbf{q}} V |\mathbf{q}\rangle \langle \mathbf{q}| V^\dagger$. As is the case for the experiments shown in the next section, the summation over all computational basis can be done exactly when the number of qubits N is sufficiently small; we may compute $\lambda_{\mathbf{q}}$ from \tilde{D} and weigh $\langle \mathbf{q} | V^\dagger O V | \mathbf{q} \rangle$ accordingly to compute

$$\langle O \rangle = \text{Tr}[\rho O] \quad (18)$$

$$= \sum_{\mathbf{q}} \lambda_{\mathbf{q}} \langle \mathbf{q} | V^\dagger O V | \mathbf{q} \rangle. \quad (19)$$

When N becomes larger, this is not realistic and hence we estimate $\{\lambda_{\mathbf{q}}\}$ by stochastic sampling [55]. Namely, we measure the outcome of $\tilde{D} |0\rangle^{\otimes N}$ to obtain the approximated eigenvalue distribution up to sufficient accuracy, which improves as the square root of the number of measurement shots.

It is noteworthy to point out that such approximation process is necessary. It might seem that one may simply dephase the quantum state after the operating \tilde{D} and then measure the desired physical observable. However, this is not the case since the weight of an array of bits \mathbf{q} realized by $\tilde{D} |0\rangle$ is $\lambda_{\mathbf{q}}$, but not $\sqrt{\lambda_{\mathbf{q}}}$. Namely, the probability distribution is proportional to $\{\lambda_{\mathbf{q}}^2\}$, but not $\{\lambda_{\mathbf{q}}\}$, and therefore yield inappropriate measurement results.

Finally, we summarize the measurement scheme using N qubits as follows,

- (0. Optimize the set of variational parameters in the vector representation, i.e., using $2N$ qubits.)
1. Let \mathbf{q} be an array of N bits with nonzero probability $\lambda_{\mathbf{q}}$ and initialize the state of N qubits to $|\mathbf{q}\rangle$.
2. Measure the observable O using the quantum state with transformed basis $|\psi_{\mathbf{q}}\rangle = V |\mathbf{q}\rangle$.

3. Repeat 1 and 2 for any \mathbf{q} with nonzero probability.
4. Calculate the weighed sum as $\langle O \rangle = \sum_{\mathbf{q}} \lambda_{\mathbf{q}} \langle \psi_{\mathbf{q}} | O | \psi_{\mathbf{q}} \rangle$

where $\lambda_{\mathbf{q}}$ is replaced with the approximated distribution if necessary.

IV. RESULTS

In the following, we give demonstration of our dVQE scheme by both quantum and numerical simulations of the quantum circuit with depolarizing error. The cost function $\langle \hat{\mathcal{L}}^\dagger \hat{\mathcal{L}} \rangle$ is evaluated via sampling each Pauli term from noisy quantum circuit, whose variational parameters are optimized by the sequential minimal optimization technique [47]. The detailed procedure is provided in Appendix A. The mitigation scheme for the gate errors is also discussed in Appendix B.

As examples, the quantum Ising model and the persistent current model [56] are simulated. In both cases, we consider local dissipation such that the vector representation of the GKSL equation is given as

$$\hat{\mathcal{L}} |\rho\rangle = \left(-i(H \otimes \mathbb{1} - \mathbb{1} \otimes H^T) + \sum_a \sum_{i=0}^{N-1} \gamma_a \hat{\mathcal{D}}[c_i^{(a)}] \right) |\rho\rangle, \quad (20)$$

where the $c_i^{(a)}$ denotes the a -th jump operator, with its amplitude γ_a , acting on the i -th site.

A. Quantum Ising model

First, we compute the NESS of the quantum Ising model with transverse field under both damping and dephasing effect. The Hamiltonian for this model is defined as

$$H = \frac{1}{2} \sum_i \sigma_i^z \sigma_{i+1}^z + g \sum_i \sigma_i^x, \quad (21)$$

where H is the Hamiltonian of the model. Here, σ_i^α ($\alpha = x, y, z$) is the Pauli operator for the i -th spin and g is the amplitude of the transverse field. The jump operators, denoted as $c_i^{(1)}$ and $c_i^{(2)}$ for the damping and dephasing effect on the i -th spin respectively, are given as

$$c_i^{(1)} = \sigma_i^-, \quad (22)$$

$$c_i^{(2)} = \sigma_i^z, \quad (23)$$

with their strengths denoted as $\gamma^{(1)}$ and $\gamma^{(2)}$, respectively. The spin ladder operator is defined as $\sigma_i^\pm = (\sigma_i^x \pm i\sigma_i^y)/2$. Although the model does not show any phase transition, the competition between the Ising interaction, transverse field and dissipation gives us suitable testbed for the dVQE scheme.

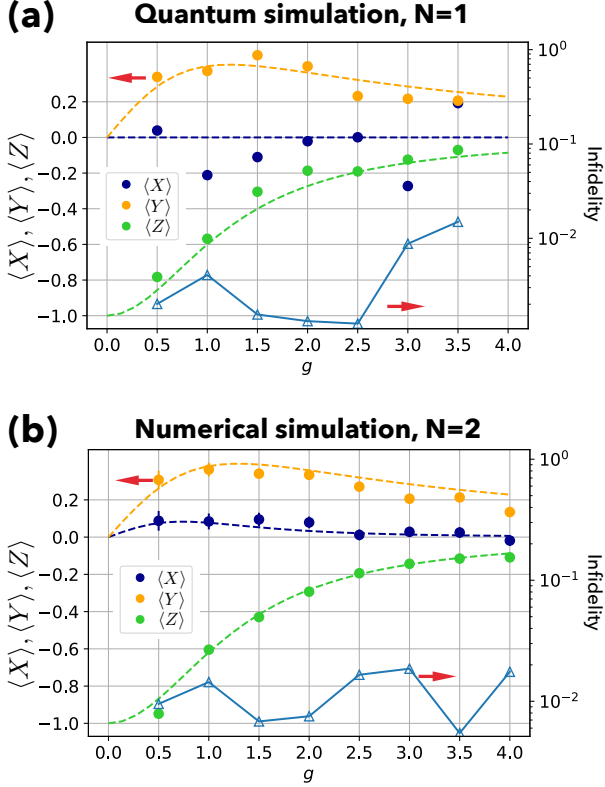


FIG. 4. (Color Online) (a) Quantum simulation and (b) numerical simulation of magnetization curves (left axis) for the dissipative quantum Ising model. The colors, blue, orange, and green, correspond to x, y, and z components of the mean magnetizations respectively for each dVQE (filled circles) and exact diagonalization (dotted lines). The unfilled triangles denote the infidelity $1 - F$ (right axis) which is typically 10^{-2} . The dissipation amplitudes are taken as $\gamma_1 = 1$ and $\gamma_2 = 0.5$. The eigenvalue distribution ansatz is decoupled (entangled) types shown pictorially in Fig. 2(b) (Fig. 2(a)) with the repetition numbers taken as $D_1 = D_2 = 1$ ($D_2 = 0$) for system size $N = 1(2)$ under quantum (numerical) simulation. Each Pauli term is sampled over 400 times.

Figure 4 shows the magnetization curves of the NESS with the dissipation amplitudes taken as $\gamma_1 = 1$, $\gamma_2 = 0.5$. The evaluation of the quantities is carried out by sampling with gate error mitigation for both the optimization and observable measurement procedure in the quantum and numerical simulation. From the density matrix obtained by the exact diagonalization and the dVQE scheme, the infidelity is calculated as $1 - F$ where the fidelity F between the two matrices, denoted as ρ_1 and ρ_2 , respectively, is given as

$$F = \left(\text{Tr} \sqrt{\sqrt{\rho_{\text{ED}}} \rho_{\text{dVQE}} \sqrt{\rho_{\text{ED}}}} \right)^2. \quad (24)$$

While the infidelity, which qualifies the accuracy of the optimized ansatz, is typically in the order of 10^{-2} , the deviation of the observable is relatively larger. In partic-

ular, for the quantum simulation, we observe that the sequential minimization optimization applied in this paper can find optimal parameters quite accurately irrespective of the imperfect evaluation of the cost function.

B. Coupled QED cavities with persistent current

Another good candidate for the demonstration of the dVQE scheme is the effective model of coupled QED cavities in the limit of very strong repulsion, whose Hamiltonian is given as

$$H = \sum_i (J \sigma_i^+ \sigma_{i+1}^- + \lambda \sigma_i^+ \sigma_{i+1}^+ + \text{h.c.}) + \mu \sigma_i^+ \sigma_i^-, \quad (25)$$

where J and λ correspond to the tunable coupling between adjacent cavities and μ is the chemical potential which originates in the energy offset by the local repulsion of the photons. In the following, we take the chemical potential as the scale of energy, i.e., $\mu = 1$, and fix $J = \lambda = 0$. It is proposed in Ref. [56] that, by appropriately engineering the interaction between the reservoir and the cavities, one may induce two-site dissipations that give rise to non-equilibrium current. Together with the damping and dephasing, we take such decoherence into account as

$$\begin{aligned} c_i^{(1)} &= \sigma_i^-, \\ c_i^{(2)} &= \sigma_i^z, \\ c_i^{(3)} &= \alpha \sigma_i^- + \beta \sigma_i^+ + \gamma \sigma_{i+1}^- + \delta \sigma_{i+1}^+. \end{aligned} \quad (26)$$

The engineered dissipation, denoted as $c_i^{(3)}$, consists of four terms, and hence we set $\gamma^{(3)} = 1$ for simplicity. To reduce the number of parameters, we set the parameters as $\alpha = \gamma^* = \cos \theta$ and $\delta = \beta^* = \sin \theta$. In the following, we investigate the circulating current,

$$\mathcal{I}_i^\eta = -\eta \sigma_i^+ \sigma_{i+1}^- + \text{h.c.}, \quad (27)$$

where $\eta = |\alpha|^2 - |\delta|^2 = \cos^2 \theta - \sin^2 \theta$. This reservoir-engineering induced current does not vanish in the thermodynamic limit in contrast to the gauge-flux induced currents and also expected to be robust in the presence of perturbations.

The numerical simulation of the persistent current is shown in Fig. 5. The persistent current creates an excitation on one site while destroying at the neighboring site, accurate evaluation of quantum entanglement is required compared to the case in the dissipative quantum Ising model. We find that the higher computational cost is required to obtain more accurate description of the non-equilibrium flow.

V. CONCLUSION

We have proposed the variational quantum algorithm to obtain the non-equilibrium steady state

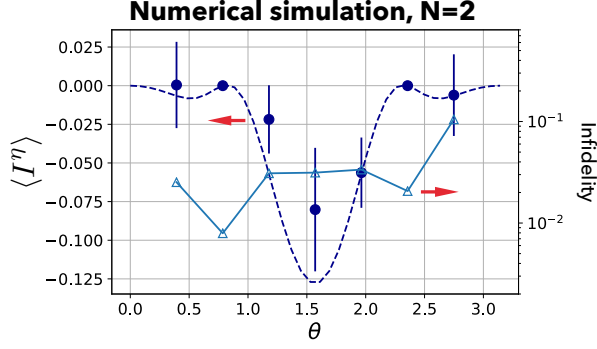


FIG. 5. (Color Online) Numerical simulation of the persistent current (left axis) and infidelity (right axis) for the reservoir-engineered coupled QED model. The blue filled circles and dashed line are the persistent current calculated by the dVQE scheme and exact diagonalization, and the unfilled triangles denote the infidelity. The dissipation amplitudes are taken as $\gamma_1 = 0.3$ and $\gamma_2 = 0.5$ for damping and dephasing, respectively. We employ the entangled type for the eigenvalue distribution ansatz, and take the repetition numbers as $D_1 = D_2 = 2$. Each Pauli term is sampled over 400 times.

(NESS) of an open quantum many-body system, named the dissipative-system Variational Quantum Eigensolver (dVQE). Our dVQE scheme, based on the quantum-classical hybrid algorithm that are intended to compute the eigenstates and their eigenenergies of a given Hamiltonian, optimizes the variational parameters of the ansatz for the NESS by minimizing the cost function defined from the time evolution generator of the quantum master equation. Also a measurement scheme for the physical observables that characterize the quantum state has been included.

The demonstration of the dVQE scheme is given by both quantum and numerical simulations. In the former, we have used the actual quantum device provided in Rigetti Quantum Cloud Service, and in the latter we have performed numerical simulations for noisy quantum circuits. It is shown that the magnetization in dissipative quantum Ising model and non-equilibrium current in reservoir-engineered coupled QED cavity model can be simulated by the dVQE scheme. We believe that the current work extends the applicability of the VQE to investigate the intriguing yet challenging field; quantum simulations with considerably large number of qubits would have the potential of exploring the wide spectrum of open quantum system.

ACKNOWLEDGEMENTS

We are grateful to Ryusuke Hamazaki for fruitful discussions. This work was supported by QunaSys and MEXT Q-LEAP. Quantum circuits were numerically simulated with a variational quantum circuit simulator Qulacs [45]. The actual quantum simulations were per-

formed on the device provided by the Rigetti Quantum Cloud Service [46].

N. Y. was supported by the JSPS through Program for Leading Graduate Schools (ALPS) and JSPS fellowship (JSPS KAKENHI Grant No. JP17J00743). K. M. thanks METI and IPA for its support through MITOU Target program. K. M. is also supported by JSPS fellowship (JSPS KAKENHI Grant No. JP19J10978). K. F. is supported by KAKENHI Grant No. JP16H02211, JST PRESTO JPMJPR1668, JST ERATO JPMJER1601, and JST CREST JPMJCR1673, MEXT Q-LEAP JPMXS01180673.

Appendix A: Optimization of variational parameters

In this Appendix, we discuss the quantum-classical hybrid optimization of the parametrized quantum circuit for the vector representation of the NESS in open quantum system. Let R_d (R_v) be the number of parameters for the diagonal matrix D (basis transformation V) in the variational quantum circuit that is expressed as

$$U(\theta) = [V(\theta_v) \otimes V^*(\theta_v)] \tilde{D}(\theta_d), \quad (\text{A1})$$

where $\theta := \{\theta_d^r\}_{r=1}^{R_d} \cup \{\theta_v^r\}_{r=1}^{R_v}$ is the set consisting of the total $R = R_d + R_v$ parameters.

As is discussed in Sec. III, the cost function is defined as

$$C(\theta) := \langle 0 | U^\dagger(\theta) \mathcal{L}^\dagger \mathcal{L} U(\theta) | 0 \rangle, \quad (\text{A2})$$

where \mathcal{L} denotes the vector representation of the Lindblad operator. we may apply the sequential minimal optimization (SMO) technique [47]. This method, explicitly taking advantage of the periodicity of the cost function with respect to the parameters, has been shown to work very efficiently when one has access to the exact expectation values. The concrete algorithm of the SMO used in our work is given as follows:

1. Initialize the variational parameters as $\theta_{n=0}$ where n is the number of the update steps already performed.
2. Choose the index $r_n \in \{1, \dots, R\}$ for the parameter to be optimized. This is done in a sequential manner.
3. With the QPU, estimate the s -th point of the landscape, $C_n(\theta_{n,s})$, whose parameters are given as

$$\begin{aligned} \theta_{n,s} = & \{\theta_n^{(1)}, \dots, \theta_n^{(r-1)}, \\ & s \left(\theta_{\max}^{(r)} - \theta_{\min}^{(r)} \right) / N_s, \\ & \theta_n^{(r+1)}, \dots, \theta_n^{(R)}\}, \end{aligned} \quad (\text{A3})$$

where $\theta_{\max}^{(r)}$ and $\theta_{\min}^{(r)}$ are the maximum and minimum of the variational parameter determined from the periodicity and restriction. Here, N_s is the number of function evaluation per parameter.

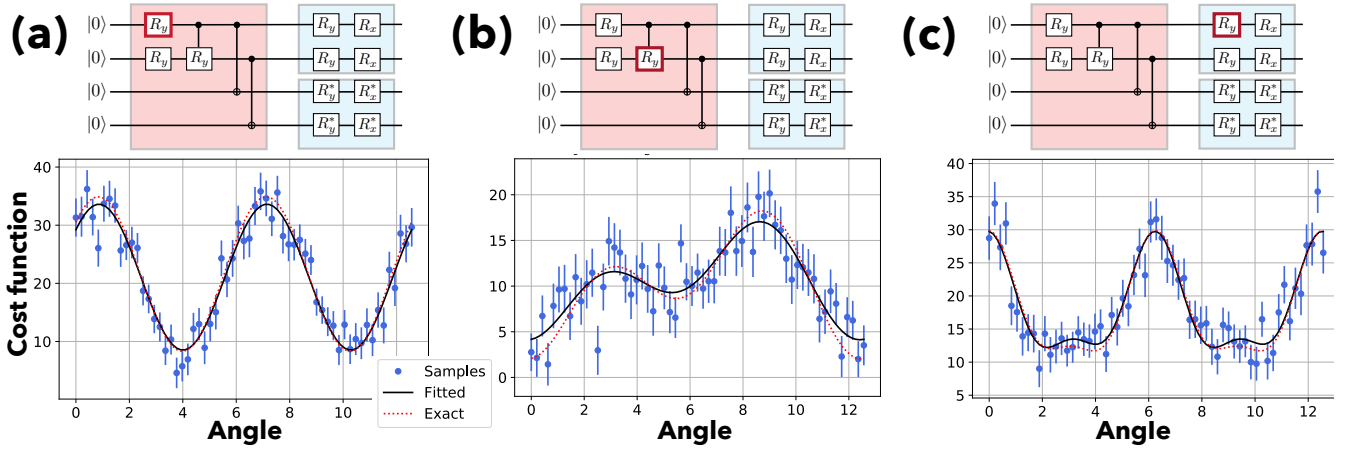


FIG. 6. (Color Online) Numerical simulation for the landscape of the cost function with respect to single rotational angle for (a) the RY gate in \tilde{D} , (b) the controlled RY gate in \tilde{D} , and (c) the RY gate in V . The blue dots are the error mitigated value obtained by sampling from noisy quantum circuits, the black lines obtained from fitting into function with appropriate modes, and the red line is the exact value. The Liouvillian operator is identical to the one employed in Sec. IV B with the parameters given as $J = 0.3, \lambda = 0, \mu = 1, \gamma_1 = 0.3, \gamma_2 = 0.5, \theta = \pi/8$. We take entangled type for the eigenvalue distribution ansatz with the repetition numbers $D_1 = D_2 = 1$. Each Pauli term is sampled over 400 times.

4. With the CPU, perform the curve fitting and determine the optimal value $\theta^{(r)}$ that the minimizes the cost function. Replace the previous $\theta_n^{(r)}$ with the optimal value to define the updated parameters θ_{n+1} .
5. Repeat 2-4 until the optimization converges.

The periodicity plays important role during the step 4 in the above algorithm. Shown in Fig. 6 is the comparison between the cost function landscapes calculated exactly and the one estimated from sampled points. While the parameters for usual rotational gates exhibit period 2π , as in the panel (a), parameters for controlled rotation gates (panel (b)) or the basis transformation (panel (c)) result in showing multiple modes [57].

Appendix B: Mitigation of gate errors

In this Appendix, we introduce the gate error mitigation scheme to obtain the ideal measurement result.

First, for the quantum simulation using the real quantum device provided in Rigetti Quantum Cloud Service, we consider quantum circuits with redundant structure to increase the noise [58].

Among the most fundamental gate sets employed in the current quantum device, namely $R_z(\phi)$ with arbitrary ϕ , $R_x(\pm\pi/2)$, and the control Z (CZ) gates, the main noise sources are known to be the latter two. We therefore consider replacing the gates using the following

identities for a positive odd integer $\mathcal{E} \in \{1, 3, 5, \dots\}$ as,

$$R_x(\pm\pi/2) \equiv R_z(\pi) (R_x(\pm\pi/2))^{\mathcal{E}} R_z(\pi),$$

$$CZ \equiv CZ^{\mathcal{E}}.$$

Since the error for the measurement result with a given \mathcal{E} can be expected to become \mathcal{E} -times larger, we apply the linear extrapolation to estimate the result in the clean limit [59].

Figure 7 shows the comparison of unmitigated and mitigated landscape of the cost function with respect to a specific variational parameter in the ansatz. Although the error mitigation using three points from $\mathcal{E} \in \{1, 3, 5\}$ is found to be sufficient to optimize the dissipative Ising model with $N = 1$ which use 2 qubits, investigation of larger system size would require improvement of fidelity to estimate the physical observables accurately.

For numerical simulations, in contrast, we consider one and two qubit depolarizing noise. Namely, each k -qubit gate ($k = 1, 2$) is assumed to be subject to a linear mapping that operates on a mixed state ρ as

$$\rho \mapsto \rho' = (1 - p_k)\rho + \frac{4^k - 1}{4^k} p_k \mathbb{1}, \quad (\text{B1})$$

where p_k denotes the error rate. After measurements under the error rate $p_1 = \mathcal{E} \times 10^{-3}$ and $p_2 = \mathcal{E} \times 10^{-2}$ for arbitrary single- and two-qubit gates, respectively, we perform the linear extrapolation. In this paper, we adopted three points by taking $\mathcal{E} \in \{1, 2, 3\}$ as the amplitude of the error.

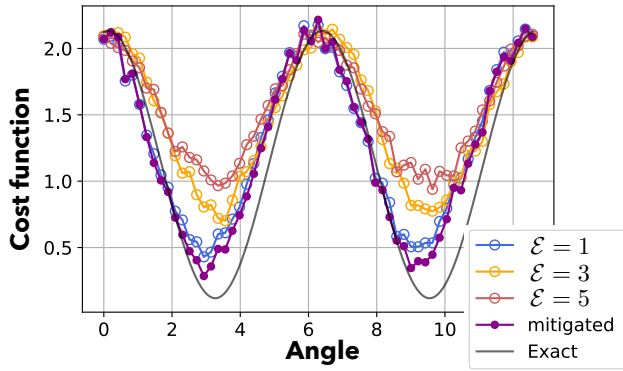


FIG. 7. (Color Online) Quantum simulation of the cost function landscape with gate error mitigation. The blue, yellow, and red unfilled circles are results from a redundant quantum circuit with $\mathcal{E} = 1, 3$, and 5 , respectively. Error mitigated values obtained from linear extrapolation are shown as the purple filled circles, and the exact values are denoted by the real line. The cost function is defined from the Liouvillian operator identical to the one in Sec. IV A with the parameters given as $g = 0.5, \gamma_1 = 1, \gamma_2 = 0.5$ with system size $N = 1$. We use the decoupled type for the eigenvalue distribution ansatz, and the repetition number for the basis transformation is $D_2 = 0$. Here, the cost function is computed for the parameter in the eigenvalue distribution, and each Pauli term is sampled over 400 times.

- [2] C. D. Bruzewicz, J. Chiaverini, R. McConnell, and J. M. Sage, *Applied Physics Reviews* **6**, 021314 (2019).
- [3] A. Aspuru-Guzik and P. Walther, *Nature Physics* **8**, 285 (2012).
- [4] J. Preskill, *Quantum* **2**, 79 (2018).
- [5] A. W. Harrow and A. Montanaro, *Nature* **549**, 203 (2017).
- [6] S. Boixo, S. V. Isakov, V. N. Smelyanskiy, R. Babbush, N. Ding, Z. Jiang, M. J. Bremner, J. M. Martinis, and H. Neven, *Nature Physics* **14**, 595 (2018).
- [7] J. Chen, F. Zhang, M. Chen, C. Huang, M. Newman, and Y. Shi, arXiv:1805.01450 (2018).
- [8] A. Bouland, B. Fefferman, C. Nirkhe, and U. Vazirani, arXiv:1803.04402 (2018).
- [9] S. Bravyi, D. Gosset, and R. Koenig, *Science* **362**, 308 (2018).
- [10] B. Villalonga, D. Lyakh, S. Boixo, H. Neven, T. S. Humble, R. Biswas, E. G. Rieffel, A. Ho, and S. Mandrà, arXiv:1905.00444 (2019).
- [11] S. Bravyi, D. Gosset, R. Koenig, and M. Tomamichel, arXiv:1904.01502 (2019).
- [12] I. M. Georgescu, S. Ashhab, and F. Nori, *Rev. Mod. Phys.* **86**, 153 (2014).
- [13] S. McArdle, S. Endo, A. Aspuru-Guzik, S. Benjamin, and X. Yuan, arXiv:1808.10402 (2018).
- [14] E. Farhi, J. Goldstone, and S. Gutmann, arXiv:1411.4028 (2014).
- [15] A. Peruzzo, J. McClean, P. Shadbolt, M.-H. Yung, X.-Q. Zhou, P. J. Love, A. Aspuru-Guzik, and J. L. O'Brien, *Nat. Commun.* **5**, 4213 (2014).
- [16] J. R. McClean, M. E. Kimchi-Schwartz, J. Carter, and W. A. de Jong, *Phys. Rev. A* **95**, 042308 (2017).
- [17] K. Nakanishi, K. Mitarai, and K. Fujii, arXiv:1810.09434 (2018).
- [18] J. I. Colless, V. V. Ramasesh, D. Dahlen, M. S. Blok, M. E. Kimchi-Schwartz, J. R. McClean, J. Carter, W. A. de Jong, and I. Siddiqi, *Phys. Rev. X* **8**, 011021 (2018).
- [19] T. Jones, S. Endo, S. McArdle, X. Yuan, and S. C. Benjamin, *Phys. Rev. A* **99**, 062304 (2019).
- [20] O. Higgott, D. Wang, and S. Brierley, *Quantum* **3**, 156 (2019).
- [21] R. M. Parrish, E. G. Hohenstein, P. L. McMahon, and T. J. Martínez, *Phys. Rev. Lett.* **122**, 230401 (2019).
- [22] A. Aspuru-Guzik, A. D. Dutoi, P. J. Love, and M. Head-Gordon, *Science* **309**, 1704 (2005).
- [23] P. J. J. O'Malley, R. Babbush, I. D. Kivlichan, J. Romero, J. R. McClean, R. Barends, J. Kelly, P. Roushan, A. Tranter, N. Ding, B. Campbell, Y. Chen, Z. Chen, B. Chiaro, A. Dunsworth, A. G. Fowler, E. Jeffrey, E. Lucero, A. Megrant, J. Y. Mutus, M. Neeley, C. Neill, C. Quintana, D. Sank, A. Vainsencher, J. Wenner, T. C. White, P. V. Coveney, P. J. Love, H. Neven, A. Aspuru-Guzik, and J. M. Martinis, *Phys. Rev. X* **6**, 031007 (2016).
- [24] A. Kandala, A. Mezzacapo, K. Temme, M. Takita, M. Brink, J. M. Chow, and J. M. Gambetta, *Nature* **549**, 242 (2017).
- [25] C. Hempel, C. Maier, J. Romero, J. McClean, T. Monz, H. Shen, P. Jurcevic, B. P. Lanyon, P. Love, R. Babbush, A. Aspuru-Guzik, R. Blatt, and C. F. Roos, *Phys. Rev. X* **8**, 031022 (2018).
- [26] Z. Cai and T. Barthel, *Phys. Rev. Lett.* **111**, 150403 (2013).
- [27] J. Cui, J. I. Cirac, and M. C. Bañuls, *Phys. Rev. Lett.* **114**, 220601 (2015).
- [28] A. H. Werner, D. Jaschke, P. Silvi, M. Kliesch, T. Calarco, J. Eisert, and S. Montangero, *Phys. Rev. Lett.* **116**, 237201 (2016).
- [29] A. Kshetrimayum, H. Weimer, and R. Orús, *Nat. Commun.* **8**, 1291 (2017).
- [30] N. Yoshioka and R. Hamazaki, *Phys. Rev. B* **99**, 214306 (2019).
- [31] M. J. Hartmann and G. Carleo, *Phys. Rev. Lett.* **122**, 250502 (2019).
- [32] A. Nagy and V. Savona, *Phys. Rev. Lett.* **122**, 250501 (2019).
- [33] F. Vicentini, A. Biella, N. Regnault, and C. Ciuti, *Phys. Rev. Lett.* **122**, 250503 (2019).
- [34] H. Weimer, *Phys. Rev. Lett.* **114**, 040402 (2015).
- [35] J. Jin, A. Biella, O. Viyuela, L. Mazza, J. Keeling, R. Fazio, and D. Rossini, *Phys. Rev. X* **6**, 031011 (2016).
- [36] J. Jin, A. Biella, O. Viyuela, C. Ciuti, R. Fazio, and D. Rossini, *Phys. Rev. B* **98**, 241108 (2018).
- [37] H. Weimer, A. Kshetrimayum, and R. Orús, arXiv:1907.07079 (2019).
- [38] S. Diehl, E. Rico, M. A. Baranov, and P. Zoller, *Nature Physics* **7**, 971 (2011).
- [39] B. Kraus, H. P. Büchler, S. Diehl, A. Kantian, A. Micheli, and P. Zoller, *Phys. Rev. A* **78**, 042307 (2008).
- [40] F. Verstraete, M. M. Wolf, and J. I. Cirac, *Nat. Phys.* **5**, 633 (2009).
- [41] Y. Dubi and M. Di Ventra, *Nano letters* **9**, 97 (2008).
- [42] X. Yuan, S. Endo, Q. Zhao, S. Benjamin, and Y. Li, arXiv:1812.08767 (2018).
- [43] S. Endo, Y. Li, S. Benjamin, and X. Yuan, arXiv:1812.08778 (2018).

- [44] Z. Hu, R. Xia, and S. Kais, arXiv:1904.00910 (2019).
- [45] E. Jones, T. Oliphant, P. Peterson, et al., “Qulacs,” (2018).
- [46] R. S. Smith, M. J. Curtis, and W. J. Zeng, arXiv:1608.03355 (2016).
- [47] K. M. Nakanishi, K. Fujii, and S. Todo, arXiv:1903.12166 (2019).
- [48] G. Lindblad, Comm. Math. Phys. **48**, 119 (1976).
- [49] V. Gorini, A. Kossakowski, and E. C. G. Sudarshan, Journal of Mathematical Physics **17**, 821 (1976).
- [50] Á. Rivas and S. Huelga, Open Quantum Systems: An Introduction, Springer-Briefs in Physics (Springer Berlin Heidelberg, 2011).
- [51] C. M. Bender, Reports on Progress in Physics **70**, 947 (2007).
- [52] S. G. Schirmer and X. Wang, Phys. Rev. A **81**, 062306 (2010).
- [53] Although the number of terms in the cost function increases rapidly due to the all-to-all connection between the physical and ancillary space, its growth is polynomial in N and thus can be sampled efficiently enough from the qubits [60].
- [54] It can be shown that the overlap in the vector representation, f , between the exact NESS and the optimized ansatz can be bounded as $1 - f^2 \geq \langle \mathcal{L}^\dagger \mathcal{L} \rangle / \delta$ where δ is the lowest non-zero eigenvalue of $\hat{\mathcal{L}}^\dagger \hat{\mathcal{L}}$.
- [55] When the decoupled type of the eigenvalue distribution ansatz is adopted, one can exactly evaluate the values from variational parameter $\theta_d = \{\theta_d^{(n)}\}_{n=1}^N$ as

$$\lambda_{\mathbf{q}} = \frac{\prod_n \cos(\theta_d^{(n)}) \tan^{a_n}(\theta_d^{(n)})}{\prod_n (\cos(\theta_d^{(n)}) + \sin(\theta_d^{(n)}))}. \quad (\text{B2})$$
- [56] M. Keck, D. Rossini, and R. Fazio, Phys. Rev. A **98**, 053812 (2018).
- [57] With K control qubits for the rotational gate, the cost function with respect to its parameter includes terms with period $2\pi, 2^2\pi, \dots, 2^{K+1}\pi$.
- [58] K. Heya, K. M. Nakanishi, K. Mitarai, and K. Fujii, arXiv:1904.08566 (2019).
- [59] K. Temme, S. Bravyi, and J. M. Gambetta, Phys. Rev. Lett. **119**, 180509 (2017).
- [60] G. Ortiz, J. E. Gubernatis, E. Knill, and R. Laflamme, Phys. Rev. A **64**, 022319 (2001).